ADVANCING EARTH AND SPACE SCIENCES

JGR Atmospheres

RESEARCH ARTICLE
10.1029/2025JD046185

Key Points:

- Transboundary dust from Mongolia contributes 21.3% and 41.2% to the total dust load in North and Northeast China, respectively
- Observed natural recovery in Mongolia (2005–2023) has reduced spring dust by 5% in North China and 13% in Northeast China
- Simulated active restoration in Mongolia (ref. Inner Mongolia of China) could reduce spring dust by 11% in North China and 19% in Northeast China

Supporting Information:

Supporting Information may be found in the online version of this article.

Correspondence to:

X. Guan,
guanxd@lzu.edu.cn

Citation:

Qiu, P., Guan, X., Huang, J., Da, P., Ding, Y., & Jin, Z. (2026). A transboundary air quality co-benefit of ecological restoration in Mongolia. *Journal of Geophysical Research: Atmospheres*, *131*, e2025JD046185. https://doi.org/10.1029/2025JD046185

Received 18 DEC 2025
Accepted 10 MAR 2026

Author Contributions:

Conceptualization: Xiaodan Guan
Data curation: Pengcheng Qiu
Formal analysis: Pengcheng Qiu
Funding acquisition: Xiaodan Guan
Investigation: Pengcheng Qiu
Methodology: Pengcheng Qiu, Pengbo Da, Yuhang Ding
Project administration: Xiaodan Guan
Software: Pengbo Da, Yuhang Ding
Supervision: Xiaodan Guan, Jianping Huang
Visualization: Pengcheng Qiu
Writing – original draft: Pengcheng Qiu
Writing – review & editing: Xiaodan Guan, Jianping Huang, Zhiyuan Jin

A Transboundary Air Quality Co-Benefit of Ecological Restoration in Mongolia

Pengcheng Qiu[1], Xiaodan Guan[1], Jianping Huang[1], Pengbo Da[1], Yuhang Ding[1], and Zhiyuan Jin[1]

[1]Collaborative Innovation Center for Western Ecological Safety, College of Atmospheric Sciences, Lanzhou University, Lanzhou, China

Abstract Transboundary dust storms, fueled by rampant desertification in Mongolia, pose a severe environmental threat to hundreds of millions of people and to sustainable development across East Asia. While ecological restoration is a recognized solution, its potential and cross-boundary benefits remain unquantified at a policy-relevant scale. Here we show that even without large-scale interventions, 67.5% of Mongolia's territory experienced a decrease in desertification severity from 2005 to 2023, yielding a net 23.0% reduction in spring dust emissions by 2023. This natural improvement alone reduced the dust column mass density over North China and Northeast China by 5.4% and 13.3%, respectively. If Mongolia had implemented proven ecological restoration measures similar to those adopted in China's Inner Mongolia during the same period, spring dust emissions could have been substantially reduced by 42.7%. This would in turn reduce spring dust pollution over North China and Northeast China by 10.6% and 18.6%, respectively. Such findings provide rigorous, evidence-based quantification that large-scale ecological restoration in Mongolia is not only a national imperative but also a critical strategy for delivering substantial transboundary air quality co-benefits, underscoring the global value of investing in sustainable land management.

Plain Language Summary Dust storms originating in Mongolia are a major environmental challenge, affecting air quality and health for hundreds of millions of people across East Asia. Specifically, our calculations show that 21.3% of the dust in North China and 41.2% in Northeast China originates from Mongolia. This study measures how changes in desertification in Mongolia impact these cross-border dust storms. We found that between 2005 and 2023, Mongolia's land naturally recovered, with desertification becoming less severe across two-thirds of the country. This natural improvement reduced the amount of dust released into the air by roughly 23%, leading to noticeably cleaner air in North and Northeast China. However, we also calculated what could happen if more active steps were taken. If Mongolia adopted ecological restoration methods similar to those already successful in China's Inner Mongolia, the positive impact would far surpass that of natural recovery alone. Our analysis shows that spring dust emissions could drop by 42.7%. Specifically, this measure would reduce dust pollution in North China by 10.6% and in Northeast China by 18.6%. These findings prove that investing in land restoration in Mongolia is not just a local benefit—it is a powerful tool for improving air quality throughout the entire region.

1. Introduction

Desertification, one of the most serious global environmental challenges, affects about one-quarter of the Earth's land area and one-fifth of the global population, threatening ecosystem stability and sustainable development (Huang et al., 2020; Li, Yang, et al., 2025; UNCCD, 1994). Preventing and reversing land degradation is not only the core objective of the United Nations Convention to Combat Desertification (UNCCD) but also a shared goal of the United Nations Framework Convention on Climate Change (UNFCCC) and the Convention on Biological Diversity (Maestre et al., 2025). Mongolia, in the arid belt of Central and East Asia, suffers severe desertification over more than three-quarters of its territory, making it a key and challenging region for global desertification prevention and control (Burrell et al., 2020; UNCCD, 2022). As a major dust source region in East Asia, Mongolia's severe land degradation has not only disrupted the local ecological balance but also exerted substantial impacts on the atmospheric environment of downwind countries (Chen et al., 2023, 2024; Piao et al., 2023). Confronted with this transboundary ecological challenge, regional collaborative governance has become an urgent necessity (Wang et al., 2025). Quantitatively elucidating the specific contribution of desertification in Mongolia to dust storms in China and its transboundary transport mechanisms is not only an urgent scientific issue to be addressed but also a critical scientific foundation for strengthening China–Mongolia cooperation in environmental governance and ecological security.

Ecological restoration represents the most effective strategy for combating desertification and mitigating dust emissions (Guan & Huang, 2024; Islam et al., 2025; Xu et al., 2022). Regional modeling indicates that desertification improvements driven by ecological restoration can reduce dust emissions by more than 40% (Zhou et al., 2020). To address increasingly severe land degradation, Mongolia launched the "1 Billion Trees" initiative in 2021, drawing on the desertification control experience from China's Inner Mongolia (Xinhua, 2024). However, although existing studies have revealed the potential of ecological restoration in reducing dust emissions, most research has focused on local or regional scales, with limited attention to its transboundary effects. The lack of quantitative assessment of its cross-border benefits hampers the mobilization of adequate international political will, financial resources, and targeted cooperation, potentially undermining the scale and effectiveness of proposed solutions.

To this end, we rigorously evaluated the sensitivity of northern China's dust storms to desertification changes in Mongolia by comparing two divergent pathways from 2005 to 2023: the observed historical trend and a modeled scenario of widespread ecological restoration. Our approach integrates reliable satellite observations with well-established atmospheric chemical models. For the restoration scenario, we adopt Inner Mongolia of China—a region sharing key ecological and climatic traits with Mongolia that has successfully implemented large-scale restoration—as a plausible model (Chan et al., 2023; Guo et al., 2021; Wang et al., 2023; Xu et al., 2024). This framework provides critical insights into the transboundary effects of land management and pinpoints the substantial potential of coordinated action in combating regional dust storms.

2. Data and Methods

2.1. Data Source

The initial and lateral boundary conditions for the WRF-Chem simulations were derived from the Final Operational Global Analysis (FNL) reanalysis data set, provided by the National Centers for Environmental Prediction (NCEP) and the National Center for Atmospheric Research (NCAR), with a spatial resolution of $1° \times 1°$ and a temporal resolution of 6 hr. The MODIS MOD13C2 product was used to extract both Normalized Difference Vegetation Index (NDVI) and Enhanced Vegetation Index (EVI), while the MODIS MOD15A2H and MCD43C3 products provided Leaf Area Index (LAI) and albedo, respectively (Didan, 2021; Myneni et al., 2021; Schaaf & Wang, 2021). All data sets were resampled to a uniform 0.05° spatial resolution using bilinear interpolation and aggregated into monthly averages. These data sets were incorporated into the WRF-Chem model to update land surface conditions, thereby enabling an assessment of the impact of desertification on dust intensity. In addition, these data sets were used to characterize the desertification status in Mongolia and to construct the Desertification Difference Index (DDI) for evaluating its spatiotemporal patterns and long-term trends.

Hourly PM_{10} concentration data from the National Air Quality Real-time Release Platform, maintained by the China National Environmental Monitoring Center, together with dust column mass density data from the Modern-Era Retrospective Analysis for Research and Applications Version 2 (MERRA-2), were used to characterize dust pollution and validate the model simulations. In addition, the MODIS Aerosol Optical Depth (AOD) product (MCD19A2CMG) was employed to evaluate the simulated atmospheric dust loading. To ensure a rigorous comparison, we extracted the "pure dust" AOD component from the raw MODIS data using the ratio of dust AOD to total AOD from MERRA-2. The ERA5 hourly reanalysis data set from the European Center for Medium-Range Weather Forecasts (ECMWF) was employed to capture the large-scale meteorological conditions associated with dust storms (Hersbach et al., 2020). Dust emissions data from the MERRA-2 data set were further used to identify and delineate the source regions of dust outbreaks (Gelaro et al., 2017).

2.2. Desertification Difference Index (DDI) Construction

The DDI assesses desertification severity by leveraging the inverse relationship between surface albedo and vegetation indices within the albedo-vegetation index feature space (Guo et al., 2022; Liu et al., 2020). Regions with high albedo and low vegetation indices are dominated by extensive bare surfaces and sparse vegetation, indicating higher desertification severity.

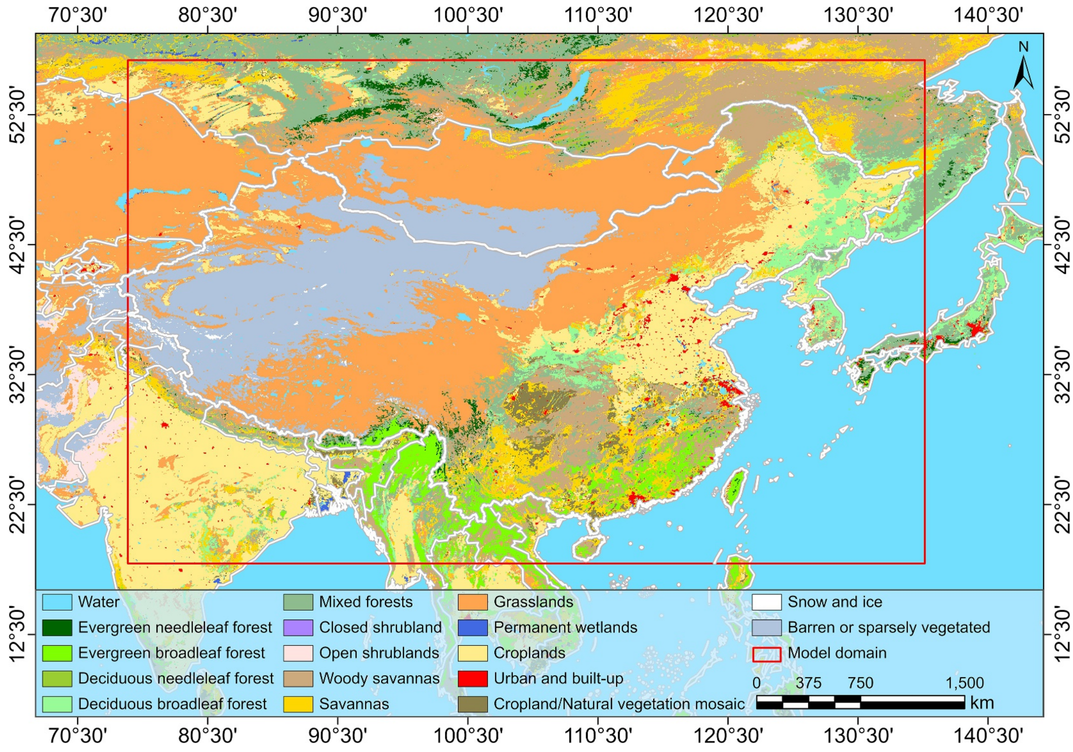

Figure 1. Spatial distribution of land use types in the study area. The red rectangle outlines the model simulation domain used in WRF experiments.

To determine the optimal vegetation index (VI) for DDI calculation in Mongolia, we conducted linear regressions between annual minimum albedo composites and annual maximum VI composites (NDVI, EVI, LAI) for 2005–2023, using data from 100 fixed randomly sampled locations. Before calculation, both the VI and albedo values were normalized to a range of 0–1 to ensure they are on the same scale. The VI yielding the strongest linear relationship was selected for subsequent analysis. The DDI was then calculated for each spatiotemporal unit using the formula:

$$\mathrm{DDI} = (-1/a) \times \mathrm{VI} - \mathrm{Albedo} \tag{1}$$

where a is the slope and VI is the vegetation index from the selected optimal regression. Higher DDI values indicate lower desertification severity.

Mongolian desertification levels were classified based on computed DDI values using the Jenks natural breaks method (Jenks, 1963). Classification accuracy was evaluated by visually interpreting the degree of desertification using high-resolution true-color Google Earth imagery for 100 randomly selected points, followed by the construction of a confusion matrix (Meng et al., 2021; Zhang et al., 2018).

2.3. Model Description and Experimental Design

This study employs the WRF-Chem model to examine the influence of desertification changes in Mongolia on the spring 2023 dust transport affecting China (Grell et al., 2005). The simulation employed a single domain covering nearly all of East Asia (Figure 1). The domain configuration and key parameterizations of physics and chemistry are shown in Table 1.

To assess the influence of actual desertification changes in Mongolia on dust storm intensity in China, and to evaluate the potential impact of implementing effective ecological restoration projects in Mongolia, we designed three sets of numerical experiments. All experiments used monthly land surface parameters, consistent with the temporal resolution at which WRF-Chem updates these variables. All modifications were strictly confined to the territory of Mongolia, and the modified model variables included GREENFRAC (based on NDVI, representing

Table 1
Physics and Chemistry Schemes Used in the WRF-Chem Model

WRF-chem	v3.9.1 (Grell et al., 2005)
Simulation domains	1
Simulation period	1 March–1 June 2023
Spin up	22 February–28 February 2023
Central Point	105.0°E, 40.0°N
Domain size	120 × 100 cells (lon × lat)
Horizontal resolution	50 km
Vertical resolution	31 eta levels up to 50 hPa
Projection	Mercator
Initial and boundary conditions	FNL

Parameterizations	Scheme	Namelist variable	Option
Physics			
Microphysics	WSM5 (Hong et al., 2004)	mp_physics	4
Radiation (long and shortwave)	RRTMG (Iacono et al., 2008)	ra_lw(sw)_physics	4
Surface model	Noah (Ek et al., 2003)	sf_surface_physics	2
Surface layer	Monin-Obukhov (Monin & Obukhov, 1954)	sf_sfclay_physics	1
Planetary boundary layer	YSU (Hong et al., 2006)	bl_pbl_physics	1
Cumulus parameterization	Grell 3D (Grell & Dévényi, 2002)	cu_physics	5
Chemistry			
Chemistry	GOCART coupled with RACM-KPP	chem_opt	301
Dust emission	Shao (2004)	dust_opt/dust_schme	4/2
Aerosol Radiative feedbacks	On	aer_ra_feedback	1

vegetation coverage), LAI12M (monthly LAI), and Albedo12M (monthly surface albedo). The first experiment (WRF_REAL) employed MODIS-based monthly land surface data from 2023 to represent the actual land surface conditions in Mongolia. The second experiment (WRF_CTL) aimed to isolate the effects of long-term land surface changes in Mongolia. This was achieved by removing the monthly linear trends of NDVI, LAI, and albedo from 2005 to 2023 at each grid point in Mongolia from the WRF_REAL inputs, thereby constructing a control scenario that excluded these long-term changes. The third experiment (WRF_REST) simulated a hypothetical scenario in which Mongolia undergoes vegetation restoration comparable to that observed in Inner Mongolia of China. To construct this scenario, we calculated the monthly linear relative trends of NDVI, LAI, and surface albedo from 2005 to 2023 for each land use type in Inner Mongolia of China (Table S1 in Supporting Information S1). These type-specific relative change rates were then applied to the corresponding land use types in Mongolia, using the WRF_CTL experiment as the baseline. By comparing WRF_REAL and WRF_CTL, we quantified the impact of observed desertification changes (2005–2023). Comparison between WRF_REST and WRF_CTL quantified the potential impact of large-scale ecological restoration. Corresponding spatial distributions of these land surface parameters under the three scenarios are shown in Figure S1 of Supporting Information S1.

Vegetation coverage data were derived from NDVI using a pixel-based binary model, a method validated by numerous studies (Li et al., 2014; Song et al., 2022). The calculation formula is as follows:

$$\mathrm{GVF}_i = \frac{\mathrm{NDVI}_i - \mathrm{NDVI}_s}{\mathrm{NDVI}_v - \mathrm{NDVI}_s} \tag{2}$$

In this context, i represents a pixel, while NDVI_s and NDVI_v correspond to the NDVI values for completely bare soil and fully vegetated pixels, respectively. In this study, NDVI_s was set to 0.05, and NDVI_v was set to 0.90.

2.4. Quantification of Mongolia's Dust Contribution to Northern China

To quantify Mongolia's contribution to dust over northern China, we employed the Shao (2004) dust emission scheme, in which the erodibility factor (EROD) defines the potential dust source regions. Two numerical experiments were conducted. The first, referred to as WRF_REAL, represents the control simulation under actual conditions. In the second experiment, all EROD values within the Mongolian territory were set to zero, effectively suppressing dust emissions from Mongolia in the model. The difference in the simulated dust column mass density between the two experiments is therefore attributed to dust originating from Mongolia.

2.5. HYSPLIT

The HYSPLIT (Hybrid Single-Particle Lagrangian Integrated Trajectory) model was employed to simulate air mass transport pathways and identify potential dust source regions (Draxler & Hess, 1998). As a Lagrangian atmospheric transport model, HYSPLIT effectively simulates the movement, dispersion, and deposition of aerosol particles in the atmosphere (Aciego et al., 2017; Dai et al., 2022; Uno et al., 2009; Yang et al., 2022). In this study, 36-hr backward trajectories were calculated at hourly intervals throughout the spring season (March–May) of 2023, using meteorological fields from the Global Data Assimilation System (GDAS) with a spatial resolution of 0.5° × 0.5°. Trajectories were initialized at 500 m above ground level for three representative receptor cities—Beijing (North China), Lanzhou (Northwest China), and Shenyang (Northeast China)—to facilitate region-specific identification of dust source areas.

To quantify the spatial contributions of dust sources, the Concentration-Weighted Trajectory (CWT) method was applied (Guan et al., 2019). For each grid cell (i, j), the CWT value (W_{ij}) was calculated as

$$W_{ij} = \frac{\sum_{k=1}^{N} C_k \tau_{ijk}}{\sum_{k=1}^{N} \tau_{ijk}} \tag{3}$$

where N is the total number of trajectories, C_k is the PM_{10} concentration associated with trajectory k, and τ_{ijk} is the residence time of trajectory k in grid cell (i, j). To reduce statistical uncertainties arising from a small number of endpoints, a weighting function $w(n_{ij})$ was applied based on the average number of endpoints per cell (avg): 1.00 ($n_{ij} > 3\text{avg}$), 0.70 ($2\text{avg} < n_{ij} \le 3\text{avg}$), 0.42 ($\text{avg} < n_{ij} \le 2\text{avg}$), and 0.17 ($n_{\text{ij}} \le \text{avg}$) (Polissar et al., 2001). Crucially, to ensure physical realism, we integrated a NDVI-based mask (springtime NDVI <0.12) and excluded water bodies using GIS data sets (Chen et al., 2024; Zhang et al., 2024). By applying this physical constraint, we filtered non-erodible regions and more accurately pinpointed the potential dust sources for representative cities across different regions of northern China.

3. Results

3.1. Mongolia Is the Dominant Transboundary Source of Severe Dust Pollution in Northern China

The spring of 2023 witnessed exceptional dust storm activity, with 13 major events affecting northern China. During seven of these episodes, PM_{10} concentrations exceeded 1,000 μg m^{-3} across multiple monitoring stations (Figure 2a). Across Northwest and North China, seasonal mean PM_{10} concentrations widely exceeded 120 μg m^{-3}, substantially surpassing the World Health Organization guideline value of 45 μg m^{-3}. Furthermore, more than 80% of monitoring stations recorded over 20 days with daily PM_{10} concentrations exceeding 150 μg m^{-3}, while specific hotspots—including southern Xinjiang, the Hexi Corridor, and western Inner Mongolia of China—experienced more than 30 such days (Figure 2c).

Due to severe desertification, Mongolia has become a major transboundary source of dust affecting North and Northeast China. MERRA-2 dust emission data indicate that strong surface winds over the desertified regions of Mongolia generated substantial dust emissions, which were transported by upper-level northwesterly winds toward North and Northeast China (Figures 2d and 2e). Concentration-Weighted Trajectory results further demonstrate that air masses passing over these desertified regions in Mongolia are highly associated with elevated PM_{10} concentrations in Beijing (representing North China) and Shenyang (representing Northeast China). As shown in Figure 3, high-intensity source areas (CWT > 80 μg/m^3) are concentrated in the Mongolian Gobi, which accounts for a spatial contribution of CWT of 62.0% and 72.9% for Beijing and Shenyang, respectively. In contrast, for Lanzhou (representing Northwest China), the high-contribution source areas are clearly located in

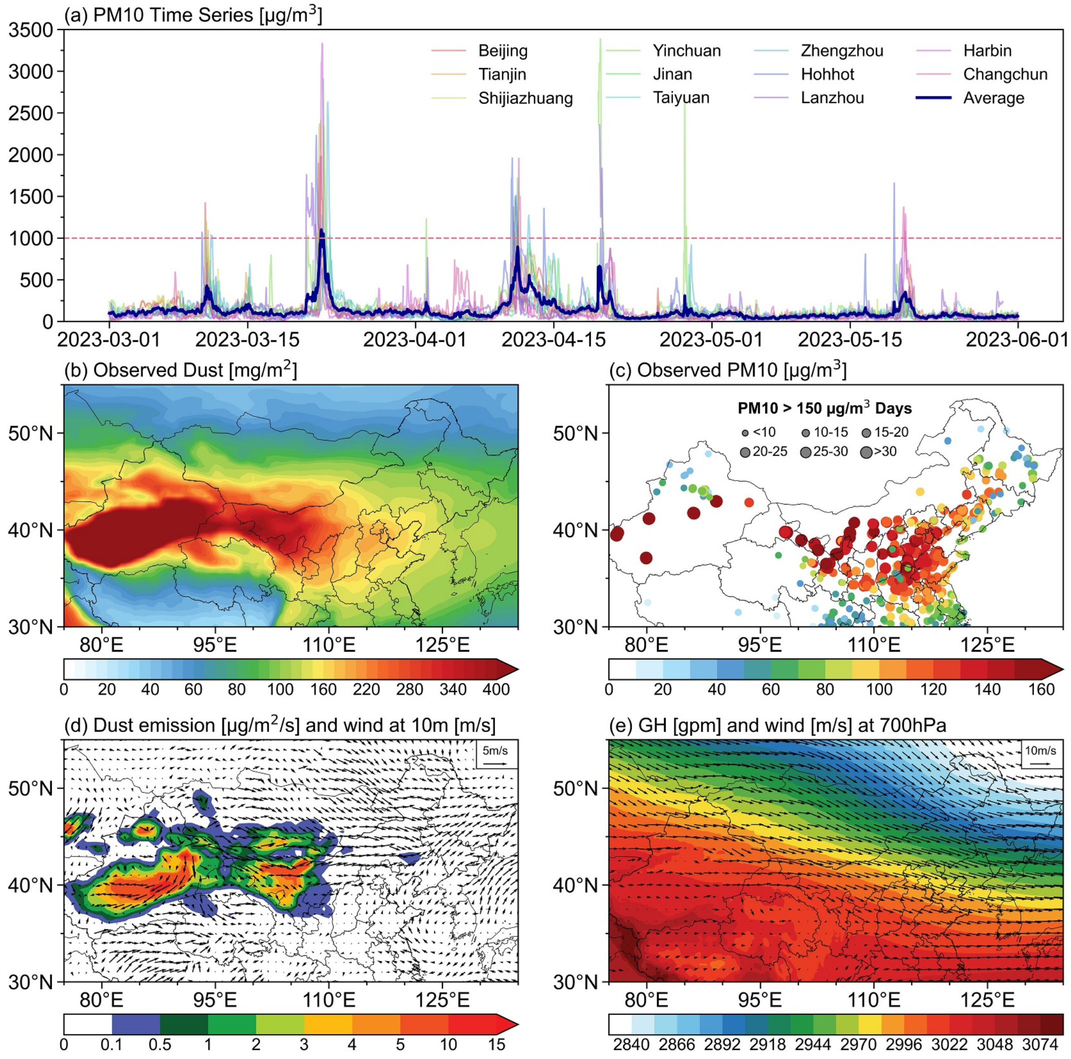

Figure 2. Dust analysis during the spring of 2023. (a) Time series of hourly PM_{10} concentrations observed at monitoring stations near major provincial capitals in northern China. The blue line represents the average PM_{10} concentration across 11 stations. (b) Spring-mean dust column mass density based on MERRA-2 data. (c) Spring-mean PM_{10} concentrations; the size of each point represents the number of days with daily average PM_{10} concentrations exceeding 150 μg/m^3. (d) Spring-mean dust emission fluxes derived from MERRA-2. (e) Spring-mean geopotential height and wind vectors at 700 hPa based on ERA5 data.

domestic deserts such as the Tengger and Badain Jaran, and the impact of Mongolian sources on Northwest China is much smaller.

Crucially, model simulations quantified Mongolia's contribution to dust in North and Northeast China, indicating that 21.3% and 41.2% of the dust in these regions, respectively, originate from Mongolia, highlighting its substantial role in the regional dust burden. By contrast, the impact of Mongolia on Northwest China was much smaller, with only 4.9% of the dust originating from Mongolia (Figure 4).

3.2. Desertification Dynamics in Mongolia Modulate Dust Emission Potential

To evaluate changes in dust source conditions in Mongolia, we constructed a DDI based on the feature space defined by the Normalized Difference Vegetation Index (NDVI, identified as the optimal vegetation index) and surface albedo (Figure S2 in Supporting Information S1; Figure 5b). Following the calculation of DDI, the desertification status across Mongolia was classified into five levels—non-desertification, slight desertification, medium desertification, serious desertification, and extremely serious desertification—using the Natural Breaks

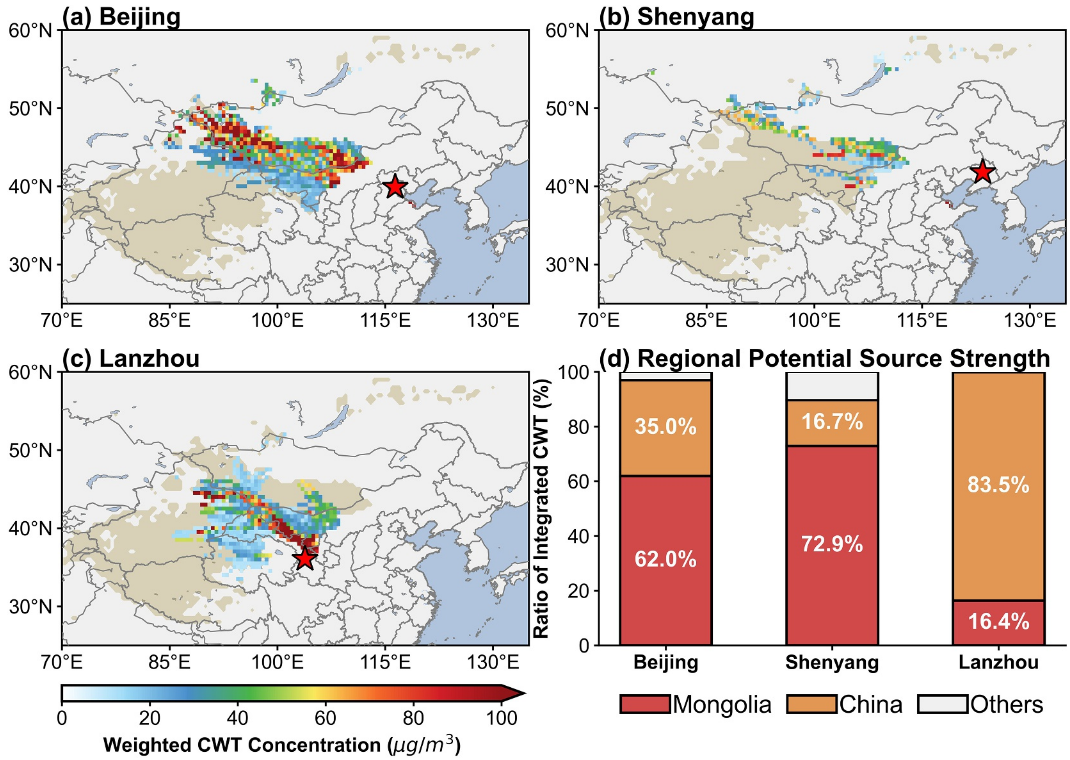

Figure 3. Identification of potential dust source regions for representative receptor sites across different regions. (a–c) Spatial distribution of the Concentration-Weighted Trajectory (CWT) for (a) Beijing, (b) Shenyang, and (c) Lanzhou during the spring of 2023. The CWT values represent the average PM_{10} concentration at the receptor site when air masses pass through a specific grid cell. A physical constraint was applied using an NDVI mask (NDVI <0.12) to isolate active dust sources and exclude non-dust-emitting surfaces. (d) Percentage spatial contribution of CWT from Mongolia (red), China (orange), and other regions (gray) for the three representative cities. Red stars on the maps indicate the geographical locations of the receptor sites.

(Jenks) classification method (Table 2) (Jenks, 1963). Validation against high-resolution imagery confirmed robust classification accuracy (Overall Accuracy = 93%, Kappa = 0.91; Figure S3 and Table S2 in Supporting Information S1).

The DDI was used to assess the spatiotemporal trends of desertification in Mongolia. At the national scale, a significant upward trend in mean DDI was observed during 2005–2023 ($p < 0.05$), indicating a moderate overall alleviation of desertification severity (Figure 5d). Spatially, the trends exhibited significant heterogeneity. While 67.5% of Mongolia's territory showed widespread improvement in desertification conditions, areas of continued degradation still existed in the southwestern and western regions.

Despite overall improvements, desertification in Mongolia remains severe because of the historically extensive land degradation. As of 2023, more than 70% of Mongolia's land area was affected by moderate or higher levels of desertification, with over 50% classified as severely or extremely desertified. Spatially, the severity of desertification in Mongolia increases from the northeast to the southwest, with the southern regions bordering China experiencing particularly severe desertification (Figure 5c). Such widespread and severe desertification results in extremely sparse vegetation and extensive exposure of loose sandy soils, creating highly favorable conditions for dust entrainment. Under strong wind events, these surface materials are readily mobilized into the atmosphere and subsequently transported by upper-level flows into North and Northeast China, contributing to frequent and intense springtime dust events.

3.3. Ecological Restoration in Mongolia Can Yield Substantial Transboundary Air Quality Benefits

An accurate and reliable regional climate model is a prerequisite for investigating the sensitivity of dust in northern China to desertification changes in Mongolia. In this study, the reliability of the WRF-Chem model was

10.1029/2025JD046185

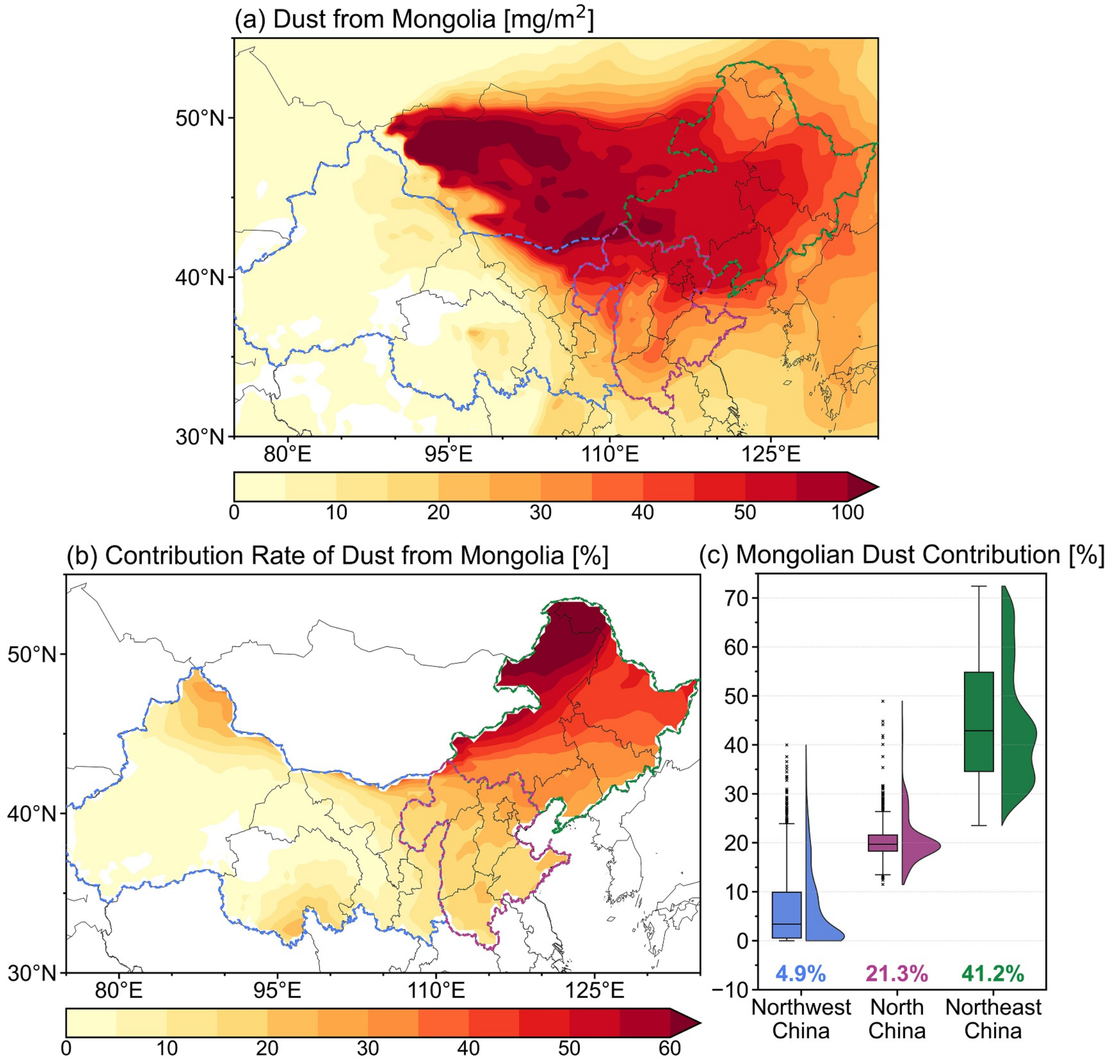

Figure 4. Contribution of dust from Mongolia to dust loading over different regions of China. (a) Spatial distribution of dust originating from Mongolia (mg m^{-2}). (b) Contribution rate of Mongolian dust to total dust concentrations across China (%). (c) Distribution of Mongolian dust contribution over Northwest, North, and Northeast China, where dust from Mongolia accounts for 4.9%, 21.3%, and 41.2% of the regional mean dust loading, respectively.

confirmed through multi-dimensional validation. First, the model accurately identified the Gobi and Taklamakan Deserts as the two primary source regions, with emission patterns highly consistent with MERRA-2 data (Figure 2d; Figure S4a in Supporting Information S1). Second, the model effectively captured the spatial distribution characteristics of surface PM_{10} concentrations ($r = 0.50$, $p < 0.01$; Figure S4b in Supporting Information S1). Furthermore, the simulated dust AOD showed high spatial consistency with MODIS-derived pure dust AOD ($r = 0.61$, $p < 0.01$; Figures S4c–S4e in Supporting Information S1). Combined with the simulated dust column mass density (Figure 6a), whose dust belt distribution is highly consistent with that in MERRA-2 (Figure 2b), these results reflect the model's robust capability in characterizing atmospheric column loading and regional transport processes. Therefore, the WRF-Chem model is suitable for assessing the impacts of desertification changes in Mongolia on dust over northern China.

The comparison between WRF_REAL and WRF_CTL quantitatively reveals the net dust effect of desertification changes in Mongolia during the period from 2005 to 2023. The results show that, although dust emissions increased in localized areas of western Mongolia due to desertification degradation, the substantial emission reductions in restoration regions dominated the overall trend, resulting in a net decrease of 23% in Mongolia's total dust emissions. This led to a significant reduction in dust column mass density over downwind regions, with decreases of 5.4% in North China and 13.3% in Northeast China (Figures 6b and 6c).

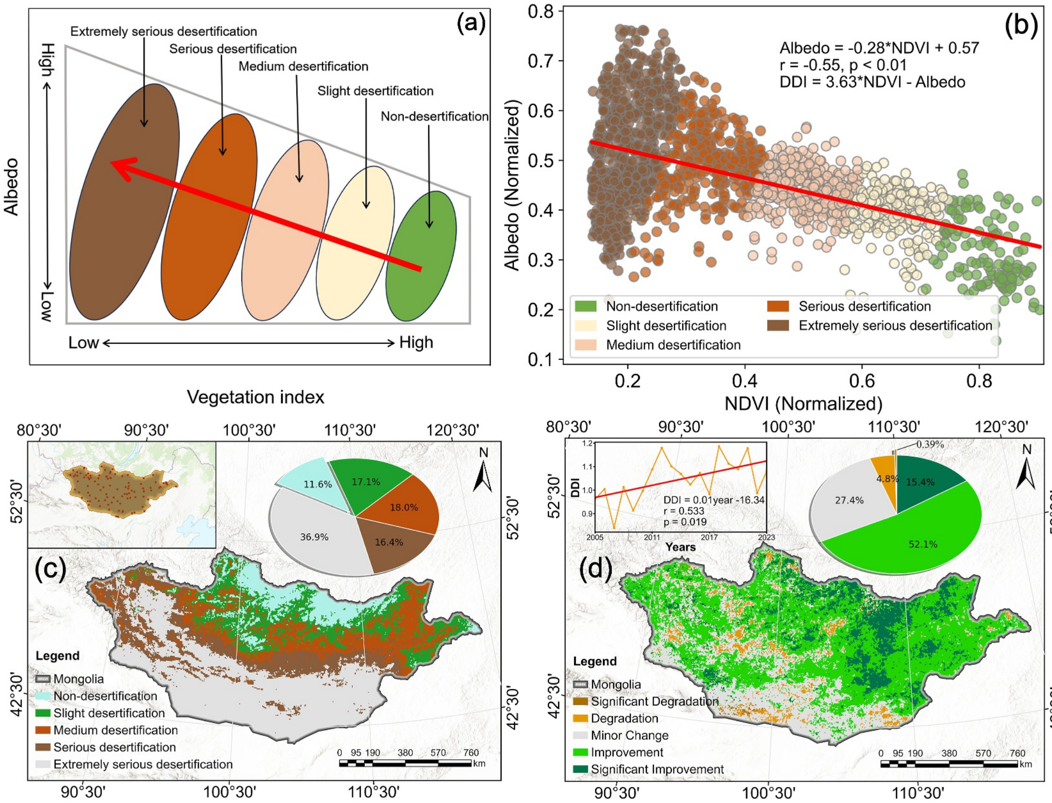

Figure 5. Spatial distribution and trend of desertification in Mongolia. (a) Albedo-Vegetation index feature space. (b) Linear fitting results between normalized NDVI and normalized Albedo, with point colors representing desertification levels. (c) Spatial distribution of desertification in Mongolia in 2023, with red points on the top-left map indicating random sampling points used for constructing the Desertification Difference Index. (d) Trends in desertification in Mongolia from 2005 to 2023, with the inset in the top-left corner showing the regional average time series.

In contrast to the slower and spatially uneven recovery in Mongolia, China's Inner Mongolia has achieved faster and more widespread restoration through large-scale ecological rehabilitation efforts (Figure 7, Table S1 in Supporting Information S1). The comparison between WRF_REST and WRF_CTL simulates the potential outcome if Mongolia were to achieve vegetation restoration at a rate comparable to that of Inner Mongolia of China. Under this scenario, Mongolia's total dust emissions would be reduced by 42.7% (Figure 6f). As a result, the downwind dust column mass density over China would decline substantially, with reductions of 10.6% in North China and 18.6% in Northeast China (Figures 6b and 6e). These gains substantially exceed those observed under the recent natural and uneven recovery, underscoring the significant potential of coordinated ecological restoration for regional dust mitigation.

Table 2
Classification of Desertification Types Based on Desertification Difference Index Values and Analysis of Their Change Trends

DDI classification criteria		DDI trend analysis	
DDI range	Type of desertification	DDI trend	Desertification change
<0.437	Extremely serious desertification	Trend < −0.003 and $p < 0.05$	Significant degradation
0.438–1.07	Serious desertification	Trend<−0.003 and $p > 0.05$	Degradation
1.071–1.703	Medium desertification	−0.003 ≤ Trend ≤ 0.003	Minor change
1.704–2.32	Slight desertification	Trend > 0.003 and $p > 0.05$	Improvement
>2.321	Non-desertification	Trend > 0.003 and $p < 0.05$	Significant improvement

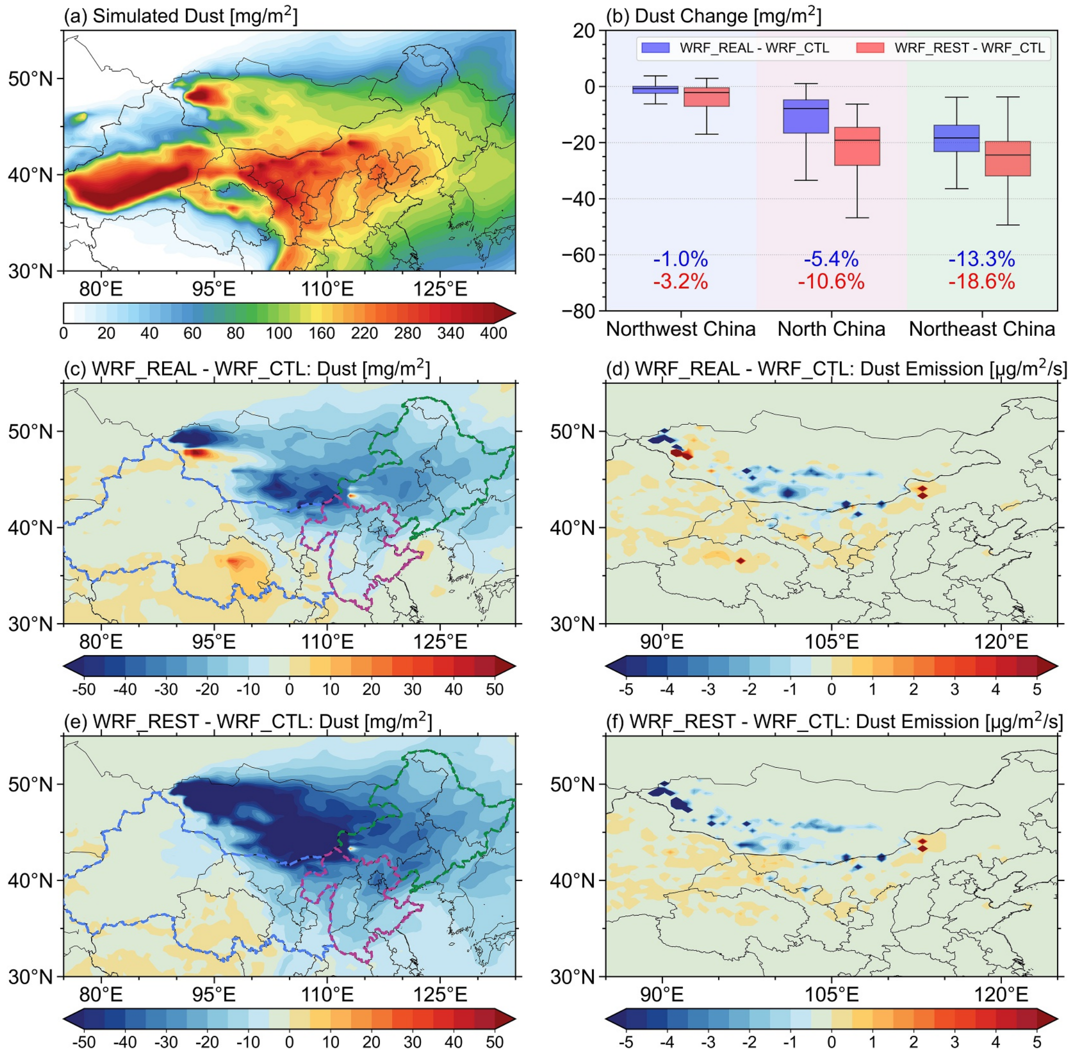

Figure 6. Impacts of desertification changes in Mongolia on spring 2023 dust column mass density over China. (a) Spring 2023 mean dust column mass density simulated using the WRF-Chem model. (b) Changes in dust column mass density over northern China under two desertification scenarios. Change rates are expressed as percentage variations in regional mean dust column mass density. (c, d) Impacts of desertification changes in Mongolia from 2005 to 2023 on spring 2023 dust column mass density and dust emission fluxes. (e, f) Changes in dust column mass density and dust emission fluxes under a scenario where vegetation in Mongolia grows at the same rate as observed in Inner Mongolia of China.

4. Conclusions and Discussion

Our study provides a quantitative and policy-relevant assessment of the transboundary air quality benefits stemming from desertification control in Mongolia. By integrating observational analysis, satellite-based desertification monitoring, and atmospheric chemistry modeling, we establish that Mongolia is among the principal sources of severe spring dust pollution affecting northern China. Crucially, we demonstrate that the observed net reduction in desertification severity over the past two decades has already yielded measurable air quality improvements downwind. Most importantly, our modeling reveals a substantial unrealized potential for dust suppression through ecological restoration, a capacity clearly demonstrated by the diverging dust-source dynamics across the border. Since the early 2000s, Inner Mongolia of China has achieved rapid human-driven recovery through large-scale initiatives such as the “Beijing-Tianjin Sandstorm Source Control Project.” By employing proven measures—including mechanical sand-fixation with straw checkerboards, the planting of drought-resistant shrubs, and strict grazing exclusion—these programs have successfully stabilized the land surface and suppressed dust emissions (Li, Chen et al., 2025; Li et al., 2023). In contrast, Mongolia's recovery has

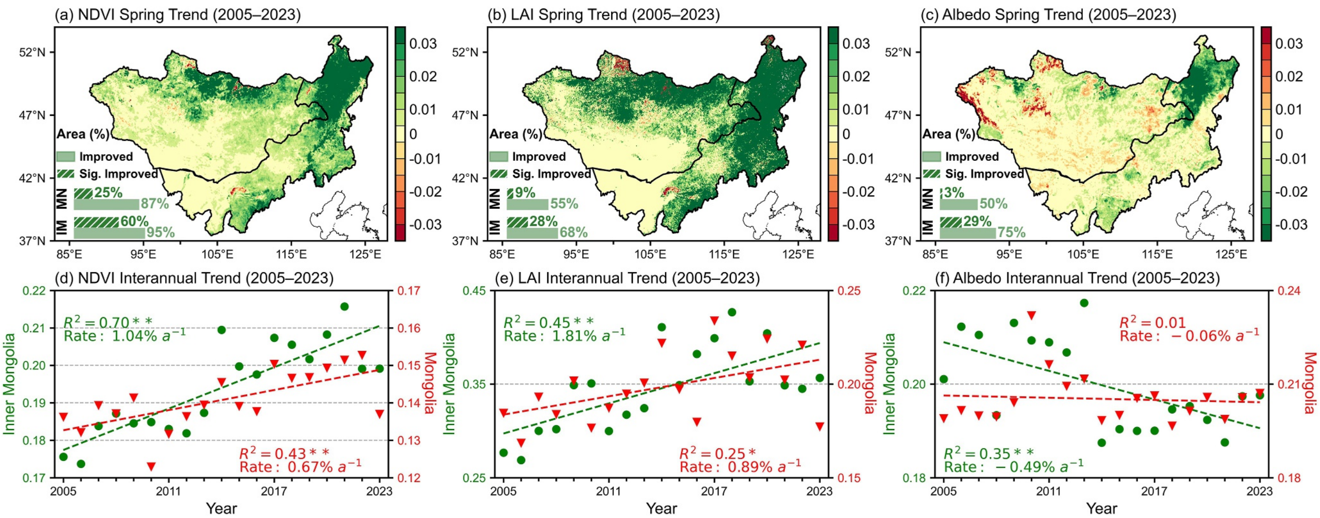

Figure 7. Spring trends of NDVI, Leaf Area Index, and surface albedo over Mongolia (MN) and Inner Mongolia of China (IM) from 2005 to 2023 were derived from MODIS products (specifically MOD13C2, MCD15A2H, and MCD43C3). Panels (a–c) present spatial trends expressed as change per decade, with inset bar charts quantifying the percentage of area showing improved (solid bars) and significantly improved (shaded bars, $p < 0.05$) conditions. Panels (d–f) show interannual variations of the corresponding variables for Inner Mongolia of China (green) and Mongolia (red), with dashed lines indicating linear regression trends. Asterisks denote the statistical significance levels: $p < 0.05$ (*) and $p < 0.01$ (**).

been hindered by intensifying overgrazing and the absence of similar institutional interventions (Chan et al., 2023). Our results suggest that implementing these same proven measures across Mongolia could nearly double the current mitigation gains, reducing total dust emissions by over 40% and substantially alleviating particulate pollution in the populous regions of North and Northeast China (Figure 8).

Our study identified Mongolia as an important source of extreme PM_{10} pollution events in North China and Northeast China. While the contribution of the classic Gobi source has been widely recognized (Mu & Fiedler, 2025; Zhu & Liu, 2024), our trajectory analysis and model simulations distinctly highlight and quantify the role of Mongolia's own degraded lands. Although satellite data show a national-scale overall improvement in vegetation, our analysis reveals that severe desertification has persisted in critical southwestern regions of Mongolia, with intensification observed in localized areas. Under the influence of strong winds, high-intensity dust emissions from these severely desertified regions are transported along major pathways, thereby maintaining high transboundary risks in downwind regions.

Due to the unique vertical stratification of dust transport in northern China, this transboundary risk poses a direct and acute threat to human health in downwind regions. Specifically, dust from the Taklimakan Desert is modulated by topography and travels primarily via high-altitude pathways, which mainly affects the total atmospheric column load (Chen et al., 2024; Feng et al., 2023). Meanwhile, other domestic dust sources in China have seen significant environmental improvement under sustained large-scale ecological restoration, leading to a continuous decline in dust emissions (Zhou et al., 2020). In contrast, land degradation in Mongolia remains severe due to the long-term effects of overgrazing and a lack of institutional restoration efforts (Zhang et al., 2024). Facilitated by frequent cyclonic activity and the absence of topographic barriers, Mongolian dust often invades North and Northeast China rapidly via low-level pathways (Huo et al., 2025). During the spring of 2023, the contribution of Mongolian sources to surface dust in North China exceeded 50%, a proportion far higher than their relative share of the total atmospheric burden (Chen et al., 2024). Consequently, Mongolian dust poses a more direct and acute threat to human health in northern China than dust from other source regions.

Our work moves beyond correlation to establish a causal chain from land management to downwind air quality. The WRF-Chem simulations quantitatively attribute a net 23% reduction in Mongolia's spring dust emissions to the observed desertification improvements between 2005 and 2023. This translated to a direct alleviation of dust loading over northern China, providing the first model-based evidence that natural recovery and local conservation efforts in Mongolia are already producing tangible cross-border co-benefits. Mongolia's current desertification reflects the 1930s U.S. Dust Bowl, which remains a benchmark for successfully reversing anthropogenic

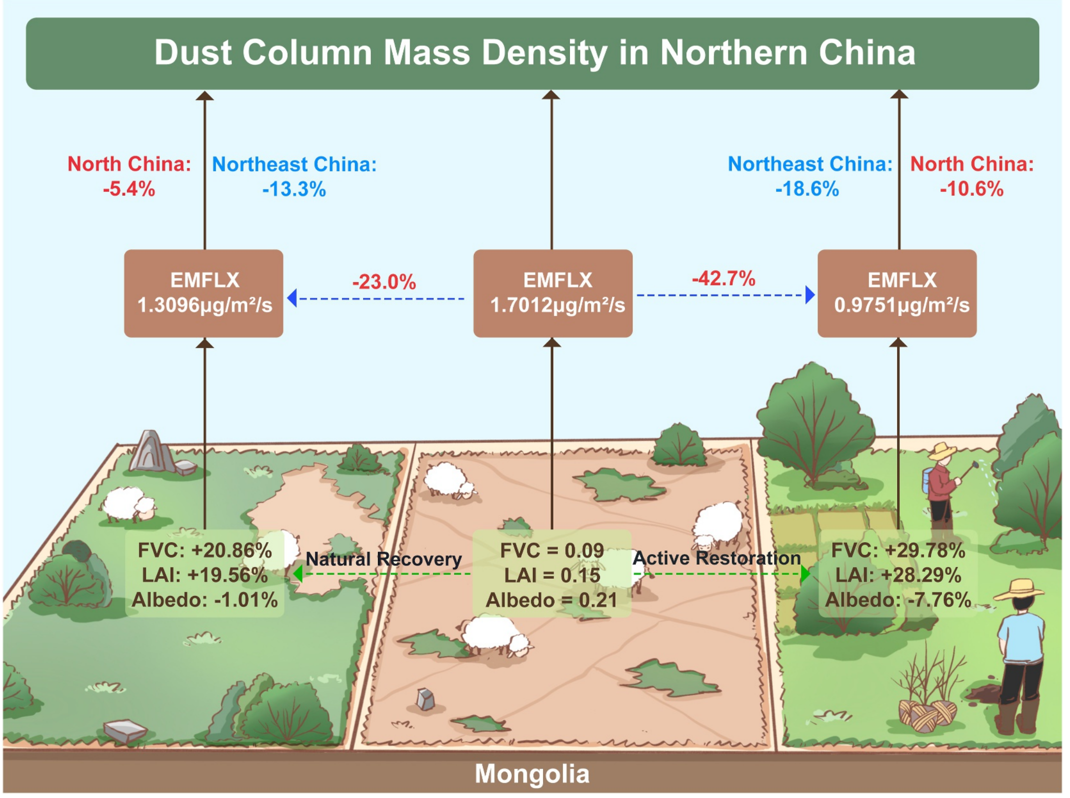

Figure 8. Impacts of different desertification change scenarios in Mongolia on dust column mass density over northern China. The middle panel represents a baseline scenario in which desertification conditions remain unchanged from 2005 to 2023, serving as a reference to assess the impacts of desertification changes. The left panel shows the actual desertification changes that occurred in Mongolia from 2005 to 2023. The right panel illustrates an ecological restoration scenario, assuming that Mongolia implements restoration measures similar to those adopted in Inner Mongolia of China. EMFLX represents surface dust emission flux. Fractional vegetation cover, Leaf Area Index, and albedo represent spring mean values, and their change rates indicate variations in these spring means.

land degradation through systemic intervention (Cook et al., 2009; McLeman et al., 2014). Historical precedents confirm the feasibility of reversing systemic land degradation. Our findings demonstrate that ecological recovery also generates substantial transboundary co-benefits. These results align with the global paradigm that sustainable land management can deliver multiple ecosystem services beyond national borders (Meyfroidt et al., 2022).

The most significant implication of our study lies in the quantified potential of large-scale, coordinated ecological restoration. The stark contrast between the dust reduction achieved under the recent uneven recovery (23%) and the potential under a scenario modeled on Inner Mongolia of China success (42.7%) reveals a massive opportunity. Inner Mongolia of China experience demonstrates that targeted, large-scale interventions can achieve faster and more extensive rehabilitation than the current pace of change in Mongolia (Chan et al., 2023; Guo et al., 2021; Wang et al., 2023; Xu et al., 2024). The "1 Billion Trees" national campaign in Mongolia thus represents a pivotal strategy not only for its domestic environmental security but also as a cornerstone for regional air quality improvement. Our results suggest that the success of this and future initiatives could prevent a significant portion of the spring dust pollution burden in northern China.

This study has certain limitations in its quantitative assessment. Specifically, the scope of research is limited to the spring of 2023. Quantitative assessments derived from a single year are inherently background-dependent; as such, they may not fully capture the full range of potential scenarios arising from the coupled fluctuations in meteorological and underlying surface conditions. However, our 46-year statistical analysis confirms that the transport pathways and source contribution shares in 2023 highly coincide with the regional long-term steady-state pattern (Figure S5 and Text S1 in Supporting Information S1). Moreover, by employing detrending techniques, we isolated the long-term ecological restoration signal from random annual anomalies in surface characteristics. This dual validation ensures that the resulting dust reduction proportions are not merely idiosyncratic to 2023 specific conditions but are scientifically robust and representative.

Conflict of Interest

The authors declare no conflicts of interest relevant to this study.

Availability Statement

The MERRA-2 data (Gelaro et al., 2017) are available from NASA (https://disc.gsfc.nasa.gov/). MODIS products, including MCD19A2CMG (Lyapustin, 2023), MOD13C2 (Didan, 2021), MOD15A2H (Myneni et al., 2021), and MCD43C3 (Schaaf & Wang, 2021), can be accessed from NASA (https://ladsweb.modaps.eosdis.nasa.gov/search/). PM_{10} data can be downloaded from https://quotsoft.net/air/. ERA5 data (Hersbach et al., 2020) are available through the Copernicus Climate Data Store (https://cds.climate.copernicus.eu/). The FNL data (NCEP, 2000), used for initializing WRF-Chem simulations, are sourced from NCEP/NCAR Reanalysis. GDAS data (NCEP, 2015), utilized for HYSPLIT trajectory analysis, can be downloaded from https://www.ready.noaa.gov/data/archives/gdas1/. WRF-Chem configurations, data processing scripts, and visualization code for this study are archived at Zenodo (https://doi.org/10.5281/zenodo.18714550) under the MIT License (Qiu et al., 2026).

Acknowledgments

This work was supported by the Fundamental and Interdisciplinary Disciplines Breakthrough Plan of the Ministry of Education of China (Grant JYB2025XDXM910), the National Key Research and Development Program of China (Grant 2024YFE0103200), the Science and Technology Department of Gansu Province (Grant 25RCKA024), and the High-Level Talent Program of Lanzhou Municipality. Additionally, it was supported by the Supercomputing Center of Lanzhou University.

References

Aciego, S. M., Riebe, C. S., Hart, S. C., Blakowski, M. A., Carey, C. J., Aarons, S. M., et al. (2017). Dust outpaces bedrock in nutrient supply to montane forest ecosystems. *Nature Communications*, *8*(1), 14800. https://doi.org/10.1038/ncomms14800

Burrell, A. L., Evans, J. P., & De Kauwe, M. G. (2020). Anthropogenic climate change has driven over 5 million km^2 of drylands towards desertification. *Nature Communications*, *11*(1), 3853. https://doi.org/10.1038/s41467-020-17710-7

Chan, F. K. S., Chen, J., Li, P., Wang, J., Wang, J., & Zhu, Y. (2023). The cross-boundary of land degradation in Mongolia and China and achieving its neutrality-challenges and opportunities. *Ecological Indicators*, *151*, 110311. https://doi.org/10.1016/j.ecolind.2023.110311

Chen, S., Zhao, D., Huang, J., He, J., Chen, Y., Chen, J., et al. (2023). Mongolia contributed more than 42% of the dust concentrations in Northern China in March and April 2023. *Advances in Atmospheric Sciences*, *40*(9), 1549–1557. https://doi.org/10.1007/s00376-023-3062-1

Chen, Y., Chen, S., Bi, H., Zhou, J., & Zhang, Y. (2024). Where is the dust source of 2023 several severe dust events in China? *Bulletin of the American Meteorological Society*, *105*(11), E2085–E2096. https://doi.org/10.1175/BAMS-D-23-0121.1

Cook, B. I., Miller, R. L., & Seager, R. (2009). Amplification of the North American "Dust Bowl" drought through human-induced land degradation. *Proceedings of the National Academy of Sciences*, *106*(13), 4997–5001. https://doi.org/10.1073/pnas.0810200106

Dai, G., Sun, K., Wang, X., Wu, S., E, X., Liu, Q., & Liu, B. (2022). Dust transport and advection measurement with spaceborne lidars ALADIN and CALIOP and model reanalysis data. *Atmospheric Chemistry and Physics*, *22*(12), 7975–7993. https://doi.org/10.5194/acp-22-7975-2022

Didan, K. (2021). MODIS/Terra vegetation indices monthly L3 global 0.05Deg CMG V061 [Dataset]. *NASA EOSDIS Land Processes Distributed Active Archive Center*. https://doi.org/10.5067/MODIS/MOD13C2.061

Draxler, R. R., & Hess, G. D. (1998). An overview of the HYSPLIT_4 modelling system for trajectories. *Australian Meteorological Magazine*, *47*(4), 295–308. https://doi.org/10.1071/es98032

Ek, M. B., Mitchell, K. E., Lin, Y., Rogers, E., Grunmann, P., Koren, V., et al. (2003). Implementation of Noah land surface model advances in the National Centers for Environmental Prediction operational mesoscale Eta model. *Journal of Geophysical Research*, *108*(D22). https://doi.org/10.1029/2002JD003296

Feng, T., Yuan, T., Cao, J., Wang, Z., Zhi, R., Hu, Z., & Huang, J. (2023). The influence of dust on extreme precipitation at a large city in North China. *Science of the Total Environment*, *901*, 165890. https://doi.org/10.1016/j.scitotenv.2023.165890

Gelaro, R., McCarty, W., Suárez, M. J., Todling, R., Molod, A., Takacs, L., et al. (2017). The modern-era retrospective analysis for research and applications, version 2 (MERRA-2). *Journal of Climate*, *30*(14), 5419–5454. https://doi.org/10.1175/JCLI-D-16-0758.1

Grell, G. A., & Dévényi, D. (2002). A generalized approach to parameterizing convection combining ensemble and data assimilation techniques. *Geophysical Research Letters*, *29*(14), 38-1. https://doi.org/10.1029/2002GL015311

Grell, G. A., Peckham, S. E., Schmitz, R., McKeen, S. A., Frost, G., Skamarock, W. C., & Eder, B. (2005). Fully coupled "online" chemistry within the WRF model. *Atmospheric Environment*, *39*(37), 6957–6975. https://doi.org/10.1016/j.atmosenv.2005.04.027

Guan, Q., Yang, Y., Luo, H., Zhao, R., Pan, N., Lin, J., & Yang, L. (2019). Transport pathways of PM10 during the spring in Northwest China and its characteristics of potential dust sources. *Journal of Cleaner Production*, *237*, 117746. https://doi.org/10.1016/j.jclepro.2019.117746

Guan, X., & Huang, J. (2024). Constructing semi-arid ecological barriers to prevent desertification. *The Innovation Geoscience*, *2*(2), 100067. https://doi.org/10.59717/j.xinn-geo.2024.100067

Guo, B., Wei, C., Yu, Y., Liu, Y., Li, J., Meng, C., & Cai, Y. (2022). The dominant influencing factors of desertification changes in the source region of Yellow River: Climate change or human activity? *Science of the Total Environment*, *813*, 152512. https://doi.org/10.1016/j.scitotenv.2021.152512

Guo, X., Chen, R., Thomas, D. S., Li, Q., Xia, Z., & Pan, Z. (2021). Divergent processes and trends of desertification in Inner Mongolia and Mongolia. *Land Degradation & Development*, *32*(13), 3684–3697. https://doi.org/10.1002/ldr.3825

Hersbach, H., Bell, B., Berrisford, P., Hirahara, S., Horányi, A., Muñoz-Sabater, J., et al. (2020). The ERA5 global reanalysis. *Quarterly Journal of the Royal Meteorological Society*, *146*(730), 1999–2049. https://doi.org/10.1002/qj.3803

Hong, S. Y., Dudhia, J., & Chen, S. H. (2004). A revised approach to ice microphysical processes for the bulk parameterization of clouds and precipitation. *Monthly Weather Review*, *132*(1), 103–120. https://doi.org/10.1175/1520-0493(2004)132<0103:ARATIM>2.0.CO;2

Hong, S. Y., Noh, Y., & Dudhia, J. (2006). A new vertical diffusion package with an explicit treatment of entrainment processes. *Monthly Weather Review*, *134*(9), 2318–2341. https://doi.org/10.1175/MWR3199.1

Huang, J., Zhang, G., Zhang, Y., Guan, X., Wei, Y., & Guo, R. (2020). Global desertification vulnerability to climate change and human activities. *Land Degradation & Development*, *31*(11), 1380–1391. https://doi.org/10.1002/ldr.3556

Huo, Q., Yin, Z., Ma, X., & Wang, H. (2025). Distinctive dust weather intensities in North China resulted from two types of atmospheric circulation anomalies. *Atmospheric Chemistry and Physics*, *25*(3), 1711–1724. https://doi.org/10.5194/acp-25-1711-2025

Iacono, M. J., Delamere, J. S., Mlawer, E. J., Shephard, M. W., Clough, S. A., & Collins, W. D. (2008). Radiative forcing by long-lived greenhouse gases: Calculations with the AER radiative transfer models. *Journal of Geophysical Research*, *113*(D13). https://doi.org/10.1029/2008JD009944

Islam, W., Zeng, F., Siddiqui, J. A., Zhihao, Z., Du, Y., Zhang, Y., et al. (2025). Combating desertification: Comprehensive strategies, challenges, and future directions for sustainable solutions. *Biological Reviews*, *100*(4), 1594–1614. https://doi.org/10.1111/brv.70015

Jenks, G. F. (1963). Generalization in statistical mapping. *Annals of the Association of American Geographers*, *53*(1), 15–26. https://doi.org/10.1111/j.1467-8306.1963.tb00429.x

Li, C., Chen, H., Wang, S., Yao, X., Chen, H., Guo, Y., et al. (2025). Land degradation and ecological restoration in desert steppe of Bayannur of Inner Mongolia, China. *Ecological Frontiers*, *45*(3), 689–692. https://doi.org/10.1016/j.ecofro.2025.01.007

Li, C., Gao, Z., Sun, B., Wu, J., Wang, H., & Ding, X. (2023). Ecological restoration effects of the Beijing–Tianjin sandstorm source control project in China since 2000. *Ecological Indicators*, *146*, 109782. https://doi.org/10.1016/j.ecolind.2022.109782

Li, F., Chen, W., Zeng, Y., Zhao, Q., & Wu, B. (2014). Improving estimates of grassland fractional vegetation cover based on a pixel dichotomy model: A case study in Inner Mongolia, China. *Remote Sensing*, *6*(6), 4705–4722. https://doi.org/10.3390/rs6064705

Li, G., Yang, B., Wu, G., Feng, G., Ljungqvist, F. C., Che, T., et al. (2025). Increased desertification exposure in dryland areas. *Ecological Indicators*, *179*, 114264. https://doi.org/10.1016/j.ecolind.2025.114264

Liu, Q., Zhang, Q., Yan, Y., Zhang, X., Niu, J., & Svenning, J. C. (2020). Ecological restoration is the dominant driver of the recent reversal of desertification in the Mu Us Desert (China). *Journal of Cleaner Production*, *268*, 122241. https://doi.org/10.1016/j.jclepro.2020.122241

Lyapustin, A. (2023). MODIS/Terra+Aqua AOD and water vapor from MAIAC, daily L3 global 0.05deg CMG V061 [Dataset]. *NASA Land Processes Distributed Active Archive Center*. https://doi.org/10.5067/MODIS/MCD19A2CMG.061

Maestre, F. T., Guirado, E., Armenteras, D., Beck, H. E., AlShalan, M. S., Al-Saud, N. T., et al. (2025). Bending the curve of land degradation to achieve global environmental goals. *Nature*, *644*(8076), 347–355. https://doi.org/10.1038/s41586-025-09365-5

McLeman, R. A., Dupre, J., Berrang Ford, L., Ford, J., Gajewski, K., & Marchildon, G. (2014). What we learned from the Dust Bowl: Lessons in science, policy, and adaptation. *Population and Environment*, *35*(4), 417–440. https://doi.org/10.1007/s11111-013-0190-z

Meng, X., Gao, X., Li, S., Li, S., & Lei, J. (2021). Monitoring desertification in Mongolia based on Landsat images and Google Earth Engine from 1990 to 2020. *Ecological Indicators*, *129*, 107908. https://doi.org/10.1016/j.ecolind.2021.107908

Meyfroidt, P., De Bremond, A., Ryan, C. M., Archer, E., Aspinall, R., Chhabra, A., et al. (2022). Ten facts about land systems for sustainability. *Proceedings of the National Academy of Sciences*, *119*(7), e2109217118. https://doi.org/10.1073/pnas.2109217118

Monin, A. S., & Obukhov, A. M. (1954). Basic laws of turbulent mixing in the surface layer of the atmosphere. *Contributions of the Geophysical Institute of the Academy of Sciences of the USSR*, *151*(163), e187.

Mu, F., & Fiedler, S. (2025). How much do atmospheric depressions and Mongolian cyclones contribute to spring dust activities in East Asia? *npj Climate and Atmospheric Science*, *8*(1), 51. https://doi.org/10.1038/s41612-025-00929-w

Myneni, R., Knyazikhin, Y., & Park, T. (2021). MODIS/Terra leaf area index/FPAR 8-day L4 global 500 m SIN grid V061 [Dataset]. *NASA EOSDIS Land Processes Distributed Active Archive Center*. https://doi.org/10.5067/MODIS/MOD15A2H.061

National Centers for Environmental Prediction (NCEP). (2000). NCEP FNL operational model global tropospheric analyses, continuing from July 1999 [Dataset]. *NSF National Center for Atmospheric Research*. https://doi.org/10.5065/D6M043C6

National Centers for Environmental Prediction (NCEP). (2015). NCEP GDAS/FNL 0.25 degree global tropospheric analyses and forecast grids [Dataset]. *NSF National Center for Atmospheric Research*. https://doi.org/10.5065/D65Q4T4Z

Piao, J., Chen, W., Wei, K., Cai, Q., Zhu, X., & Du, Z. (2023). Increased sandstorm frequency in North China in 2023: Climate change reflection on the Mongolian Plateau. *The Innovation*, *4*(5), 100497. https://doi.org/10.1016/j.xinn.2023.100497

Polissar, A. V., Hopke, P. K., & Harris, J. M. (2001). Source regions for atmospheric aerosol measured at Barrow, Alaska. *Environmental Science & Technology*, *35*(21), 4214–4226. https://doi.org/10.1021/es0107529

Qiu, P., Guan, X., Huang, J., Da, P., Ding, Y., & Jin, Z. (2026). qiupch2025/mongolia-restoration-air-quality-code: V1.0.3 [Software]. *Zenodo*. https://doi.org/10.5281/zenodo.18714550

Schaaf, C., & Wang, Z. (2021). MODIS/Terra+Aqua BRDF/Albedo albedo daily L3 global 0.05Deg CMG V061 [Dataset]. *NASA EOSDIS Land Processes Distributed Active Archive Center*. https://doi.org/10.5067/MODIS/MCD43C3.061

Shao, Y. (2004). Simplification of a dust emission scheme and comparison with data. *Journal of Geophysical Research*, *109*(D10). https://doi.org/10.1029/2003JD004372

Song, W., Mu, X., McVicar, T. R., Knyazikhin, Y., Liu, X., Wang, L., et al. (2022). Global quasi-daily fractional vegetation cover estimated from the DSCOVR EPIC directional hotspot dataset. *Remote Sensing of Environment*, *269*, 112835. https://doi.org/10.1016/j.rse.2021.112835

UNCCD. (1994). United Nations Convention to Combat Desertification in countries experiencing serious drought and/or desertification, particularly in Africa. United Nations Convention to Combat Desertification.

UNCCD. (2022). *National report: Mongolia country report*. United Nations Convention to Combat Desertification.

Uno, I., Eguchi, K., Yumimoto, K., Takemura, T., Shimizu, A., Uematsu, M., et al. (2009). Asian dust transported one full circuit around the globe. *Nature Geoscience*, *2*(8), 557–560. https://doi.org/10.1038/ngeo583

Wang, G., Shu, S., & Li, W. (2025). Asian dust threatens air pollution control efforts. *Science*, *390*(6772), 451. https://doi.org/10.1126/science.aeb2629

Wang, X., Ge, Q., Geng, X., Wang, Z., Gao, L., Bryan, B. A., et al. (2023). Unintended consequences of combating desertification in China. *Nature Communications*, *14*(1), 1139. https://doi.org/10.1038/s41467-023-36835-z

Xinhua. (2024). Mongolia plants 84 mln trees since 2021 to combat desertification. Retrieved from https://english.news.cn/20241009/d2e4d46b17f1404eaa062a0c780363aa/c.html

Xu, D., Wang, Y., & Wang, Z. (2022). Linking priority areas and land restoration options to support desertification control in northern China. *Ecological Indicators*, *137*, 108747. https://doi.org/10.1016/j.ecolind.2022.108747

Xu, S., Wang, J., Altansukh, O., & Chuluun, T. (2024). Spatiotemporal evolution and driving mechanisms of desertification on the Mongolian Plateau. *Science of the Total Environment*, *941*, 173566. https://doi.org/10.1016/j.scitotenv.2024.173566

Yang, K., Wang, Z., Luo, T., Liu, X., & Wu, M. (2022). Upper troposphere dust belt formation processes vary seasonally and spatially in the Northern Hemisphere. *Communications Earth & Environment*, *3*(1), 24. https://doi.org/10.1038/s43247-022-00353-5

Zhang, C. L., Li, Q., Shen, Y. P., Zhou, N., Wang, X. S., Li, J., & Jia, W. R. (2018). Monitoring of aeolian desertification on the Qinghai-Tibet Plateau from the 1970s to 2015 using Landsat images. *Science of the Total Environment*, *619*, 1648–1659. https://doi.org/10.1016/j.scitotenv.2017.10.137

Zhang, Y., Chen, Y., Chen, S., Alam, K., & Chen, J. (2024). Mongolia dust transport across borders under the background of global warming. *Global and Planetary Change*, *239*, 104509. https://doi.org/10.1016/j.gloplacha.2024.104509

Zhou, C., Fu, B., Wang, X., Yin, L., & Feng, X. (2020). The regional impact of ecological restoration in the arid steppe on dust reduction over the metropolitan area in northeastern China. *Environmental Science & Technology*, *54*(13), 7775–7786. https://doi.org/10.1021/acs.est.0c00017

Zhu, Q., & Liu, Y. (2024). The dominant factor in extreme dust events over the Gobi Desert is shifting from extreme winds to extreme droughts. *npj Climate and Atmospheric Science*, *7*(1), 141. https://doi.org/10.1038/s41612-024-00689-z